



Enhanced Microwave Absorption Performance in Sr-Modified $\text{La}_2\text{NiO}_{4\pm\delta}$ Nickelate With High Dielectric Loss

Sheng Liu¹, Yulan Cheng¹, Jun He^{2*}, Shuoqing Yan², Heng Luo³ and Lianwen Deng³

¹ College of Mechanical Engineering, Hunan Institute of Engineering, Xiangtan, China, ² College of Computational Science and Electronics, Hunan Institute of Engineering, Xiangtan, China, ³ School of Physics and Electronics, Central South University, Changsha, China

OPEN ACCESS

Edited by:

Ashok Kumar,
National Physical Laboratory (CSIR),
India

Reviewed by:

Xiaomeng Fan,
Northwestern Polytechnical University,
China
Shaohua Jiang,
Nanjing Forestry University, China
Satya Kesh Dubey,
National Physical Laboratory (CSIR),
India

*Correspondence:

Jun He
18373225367@163.com

Specialty section:

This article was submitted to
Quantum Materials,
a section of the journal
Frontiers in Materials

Received: 04 May 2020

Accepted: 21 July 2020

Published: 14 August 2020

Citation:

Liu S, Cheng Y, He J, Yan S,
Luo H and Deng L (2020) Enhanced
Microwave Absorption Performance
in Sr-Modified $\text{La}_2\text{NiO}_{4\pm\delta}$ Nickelate
With High Dielectric Loss.
Front. Mater. 7:271.
doi: 10.3389/fmats.2020.00271

This work aims to achieve the excellent microwave absorption in layered dielectric nickelate compounds. The phase, microstructure, electromagnetic properties, and microwave absorption of the Sr-modified $\text{La}_{2-x}\text{Sr}_x\text{NiO}_{4\pm\delta}$ ($x = 0, 0.3, 0.5, 0.75$) nickelates were investigated, determining and analyzing the role of Sr doping level. All compounds reveal the single tetragonal phase identified as the $I4/mmm$ space group, and the lattice parameters correlate with the doping content, evidenced by Rietveld refinement. By introducing strontium, the pronouncedly increased electronic conductivity contributes to the high dielectric loss, which gives rise to a superior attenuation ability and absorbing bandwidth. A minimum reflection loss of -21.07 dB was found in $\text{La}_{2-x}\text{Sr}_x\text{NiO}_{4\pm\delta}$ ($x = 0.75$) at a thickness of 1.9 mm, covering the effective bandwidth of 2.9 GHz. This enhanced microwave absorbing performance in nickelate shows promise in the radar absorbing field.

Keywords: electromagnetic absorbing materials, nickelate La_2NiO_4 , Sr substitution, paramagnetic behavior, dielectric loss

INTRODUCTION

With the considerable advancements of electrical communication technology, an extensive spread of ubiquitous electromagnetic interference (EMI) has caused a rising problem in both civil and military domain. Directed at this, broadband and high-efficiency microwave absorbing materials (MAMs) are urgently demanded to weaken or eliminate the unwanted electromagnetic signals for next-generation military electronics in aspects of all-electric aircraft, stealth fighter, defense security, etc. (Qi et al., 2016; Wei et al., 2018; Liu et al., 2019). Designing high-performance MAMs and applying these functionalized materials in actual operation are scientifically interesting and of technological importance. Intensive efforts have been spent on exploring popular alternatives for MAMs, involving carbonaceous absorbent (Chen et al., 2018, 2019), dielectric ceramics (Duan et al., 2016; Liao et al., 2017), conducting polymers (Wang et al., 2017), ferrite (Shen et al., 2017; Shang et al., 2018), magnetic metal (Chen et al., 2017), novel cermet (Luo et al., 2018; Feng et al., 2019), etc. Proverbially, MAMs with desirable attenuation capability covering wide-band frequency accord with two strict technological demands: reduced surface reflection and enhanced internal attenuation capability. To meet the above requirements, dielectric ceramics should stipulate a moderate permittivity and high dielectric loss. For typical design case in X-band

at a given thickness, the optimum complex permittivity ($\epsilon' - j\epsilon''$) corresponding to minimum reflection loss (RL) in dielectrics is confined to the 20-5j to 10-3j, according to the relationship between permittivity and reflection coefficient (Kong et al., 2013). Furthermore, an appropriately high electrical conductivity (ranging 0.01–100 S/m) of MAMs favors high absorption capability (Huynen et al., 2011; Bollen et al., 2013).

La_2NiO_4 nickelate with the K_2NiF_4 -type structure is an important class of dielectrics that have gained increasing attention, not only because of its attractive multifunctional applications in fuel cell cathode domain but also because of its interesting structure and electrical behavior, especially its permittivity (Rivas et al., 2004; Liu et al., 2009; Zhou et al., 2016). The room-temperature permittivity of La_2NiO_4 over 10^4 locates a wide frequency window from kHz to GHz (Krohns et al., 2009; Chouket et al., 2016a; Zhou et al., 2016). Concerning microwave absorption application, however, it is unsatisfactory that La_2NiO_4 exhibits an antiferromagnetic ordering and weakened room-temperature magnetism. As a result, this makes a large imbalance between permittivity and permeability and thus poor impedance match. Moreover, the imaginary part of permittivity is negligibly small beyond MHz, failing to achieve high dielectric loss (Krohns et al., 2009). A deep excavating of microwave dielectric loss mechanism could potentially favor the design of such system for microwave absorbing applications, if the dielectric loss is strengthened in GHz.

The exciting results have demonstrated that the partial substitution of La by Sr in La_2NiO_4 nickelate effectually improves the dielectric response, electrical conductivity, and magnetic properties by way of crystal structure manipulation, which seems to be an efficacious approach to ameliorate microwave absorbing properties. Electrically, as reported by Cava et al. (1991) and Wu and Neumeier (2003), the room-temperature conductivity in $\text{La}_{2-x}\text{Sr}_x\text{NiO}_{4\pm\delta}$ solid solution lifts significantly with increasing Sr doping level from 0 to 1. Particularly worth mentioning is that when the doping level is in excess of 0.5, the conductivity increases dramatically at least one order of magnitude. Magnetically, the substitution of Sr for La exhibits a paramagnetic characteristic and an enhanced spontaneous magnetization (Tran et al., 2013; Freeman et al., 2017). From these viewpoints, one can learn that the doping effect may also give rise to tunable electromagnetic properties and hence encouraged us to investigate the microwave absorption. For a typical example, Tho et al. (2014) studied the microwave absorption ability of Sr-doped $\text{La}_{1.5}\text{Sr}_{0.5}\text{NiO}_{4\pm\delta}$ ultrafine particles and found that it delivered an absorption peak of -36.7 dB at a thickness of 3.0 mm covering an absorption bandwidth of 1.4 GHz (9.2–10.6 GHz). However, the underlying mechanisms of dielectric responses are not fully discussed. Subsequently, they designed a magneto-dielectric composite by integration of magnetic CoFe_2O_4 nanoparticles and $\text{La}_{1.5}\text{Sr}_{0.5}\text{NiO}_{4\pm\delta}$, in order to enhance microwave loss capability (Xuan et al., 2014). The composite $0.4\text{CoFe}_2\text{O}_4$ - $0.6\text{La}_{1.5}\text{Sr}_{0.5}\text{NiO}_4$ exhibited a broadened absorption bandwidth of 2.6 GHz (13.5–16.1 GHz) at a relatively thin layer of 2.5 mm. However, studies concerning the structure

regulating electromagnetic performance in dielectric La_2NiO_4 are still limited.

In view of the above reports, we have experimentally carried out a detailed study on the microstructure, electromagnetic behavior, and microwave absorption of Sr-substituted $\text{La}_{2-x}\text{Sr}_x\text{NiO}_{4\pm\delta}$ ($x = 0, 0.3, 0.5, 0.75$). The doped nickelate is elaborated by the sol-gel method, and the relationship between the crystalline structure and electromagnetic property is emphatically investigated. The results indicate that the modified nickelate exhibits an enhanced microwave absorption performance in X-band, which further expands its applications.

EXPERIMENTAL

$\text{La}_{2-x}\text{Sr}_x\text{NiO}_{4\pm\delta}$ ($x = 0, 0.3, 0.5, \text{ and } 0.75$) oxides were synthesized by a sol-gel method. Analytical reagent grade precursors used as starting materials were $\text{La}(\text{NO}_3)_3 \cdot 6\text{H}_2\text{O}$, $\text{Sr}(\text{NO}_3)_2$, and $\text{Ni}(\text{NO}_3)_2 \cdot 6\text{H}_2\text{O}$. Citric acid was used as a chelating agent, and deionized water served as a solvent. The molar ratio of nitrate to citric acid was 1.2:1.0. Precursors weighted stoichiometrically were firstly dissolved into citric acid solution in an orderly manner and the pH value was adjusted to 7 by ammonia. Then, the precursor solution was mixed homogeneously, evaporated, and completely dried to obtain the xerogel. The obtained xerogel was ground, pre-sintered to burn out organics, and sintered at 1000°C for 4 h. Subsequently, the sintered powder was water-milled, dried, and granulated by sieving. A similar experimental procedure can be seen in previous reports (Liu et al., 2019). Prior to heating, the milled powders were mixed with 2% polyvinyl alcohol, pressed into pellets, and placed in a platinum crucible. Finally, the pellets were sintered at 1220°C for 6 h in ambient condition and cooled down slowly to room temperature. For the characterization, some pellets were used for phase, microstructure, and electrical characterization and others were crushed into particles and screened through 300–500 mesh to obtain the microparticles with a size of 30–50 μm for electromagnetic measurement. The microtopography for the as-sintered microparticles is shown in **Figure 2d**.

The crystalline phase of the sintered pellet was detected by X-ray diffraction (XRD, Philips X-pert PRO), using a Cu-K α radiation of $\lambda = 1.5406 \text{ \AA}$ (Duan et al., 2019). The crystal structure was analyzed by the Rietveld method using the GSAS program (Larson and Von Dreele, 2004). Grain structure and micromorphology of sintered pellets were checked using a scanning electron microscope (SEM, TESCAN VEGA 3), and the stoichiometric ratio was checked by matched energy dispersive X-ray spectroscopy (EDS) (Jiang et al., 2020). The bulk density of sintered pellets was measured using Archimedes' method. Resistivity measurements of bulks and composites were carried out using a precision LCR meter (TH2829C) and standard four-probe *dc* method, respectively. The magnetic hysteresis loops were characterized by a vibrating sample magnetometer (VSM, Lakeshore 7404). For electromagnetic measurement, the refined powders were homogeneously dispersed into paraffin wax with a mass fraction of 80%, and then the mixtures were pressed into a compact toroid composite with an outer diameter of 7 mm, an

inner diameter of 3.04 mm, and a thickness of 2.0 mm. Complex permeability and permittivity ($\epsilon_r = \epsilon' - j\epsilon''$ and $\mu_r = \mu' - j\mu''$) were assessed on a vector Network Analyzer (Agilent N5230A) in a frequency range of 8–18 GHz. The RL of composites was collectively calculated based on the transmission line theory from the measured complex permeability and complex permittivity (He et al., 2018; Liu et al., 2019).

$$Z_{in} = Z_0 \sqrt{\frac{\mu_r}{\epsilon_r}} \tanh \left[i \left(\frac{2\pi}{c} \right) \sqrt{\mu_r \epsilon_r} f d \right] \quad (1)$$

$$R_L \text{ (dB)} = 20 \lg \left| \frac{Z_{in} - Z_0}{Z_{in} + Z_0} \right| \quad (2)$$

where Z_{in} represents input impedance, Z_0 denotes the free-space impedance and is equal to 377Ω , f is the frequency, c represents the velocity of microwave in free space, and d corresponds to the absorber layer thickness.

RESULTS AND DISCUSSION

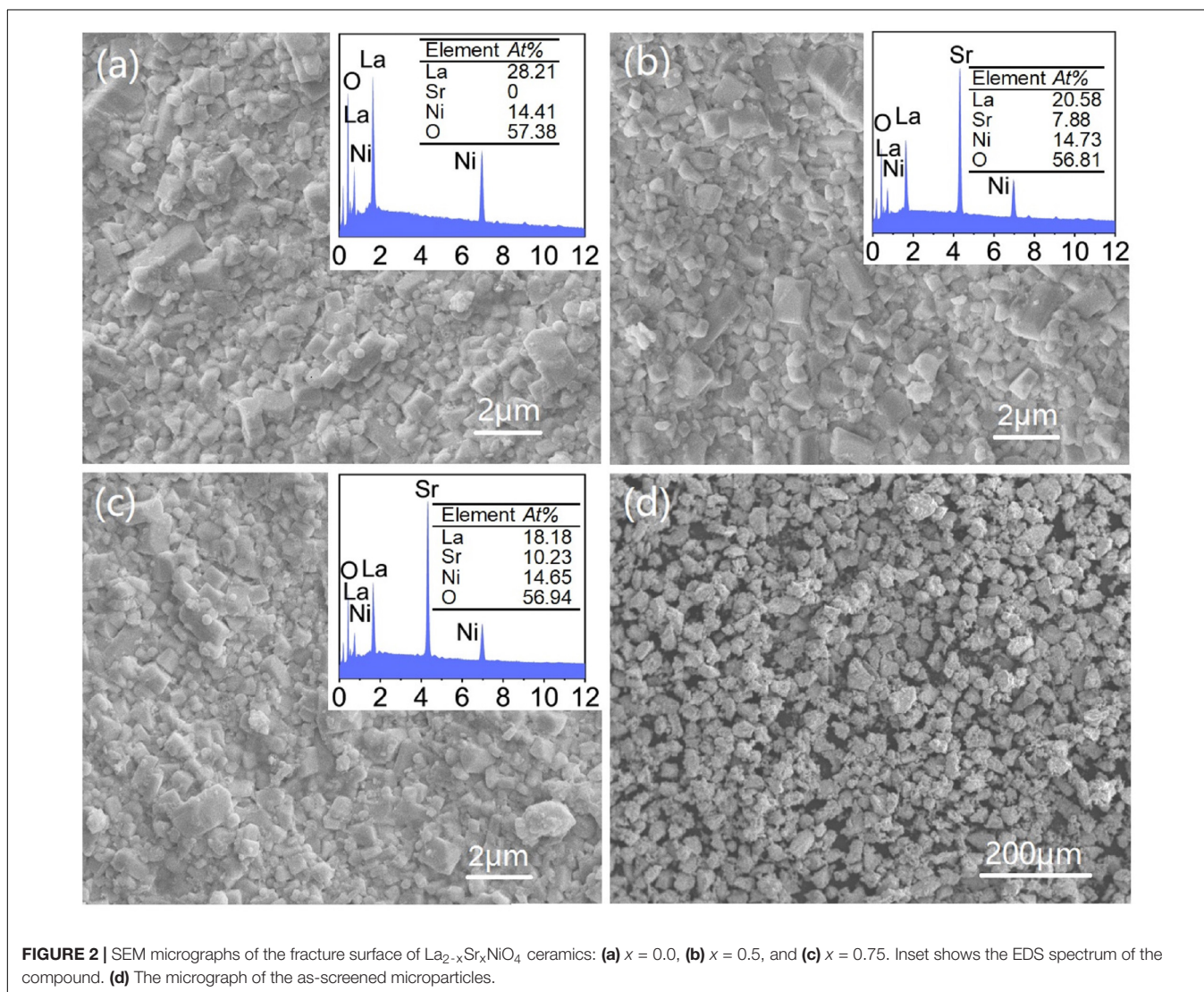
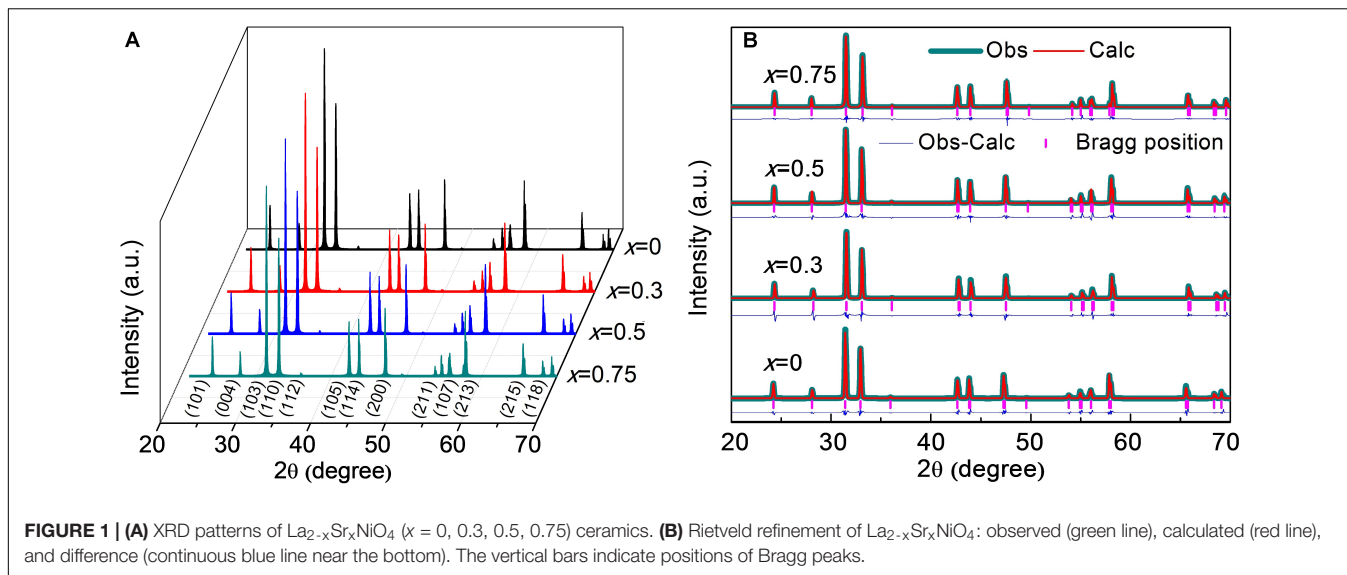
Figure 1A shows the measured XRD patterns of the undoped La_2NiO_4 and doped $\text{La}_{1-x}\text{Sr}_x\text{NiO}_{4\pm\delta}$ ($x = 0, 0.3, 0.5, 0.75$) compounds. All recorded diffraction peaks accord with the K_2NiF_4 -type structure phase, revealing the presence of a distinctive tetragonal lattice ($I4/mmm$ space group) (Ruddlesden and Popper, 1957; Ganguly and Rao, 1984). No unintentional impurity or secondary phase was discerned. For the modified counterpart, the intense diffraction peak shifts to the low angles as the Sr content increases. This result is attributed to the intercalation of partially large Sr^{2+} ions (1.31 \AA) into the small La^{3+} ion (1.216 \AA) site (Shannon, 1976), which causes an expansion of unit cell (as shown in **Table 1**). To further obtain more crystal structure information of the modified sample, Rietveld refinement was carried out using the tetragonal $I4/mmm$ model, and the refined structural parameters are given in **Table 1**. The evolution of cell parameters with Sr concentration shows the presence of crystal lattice and unit cell volume change behavior

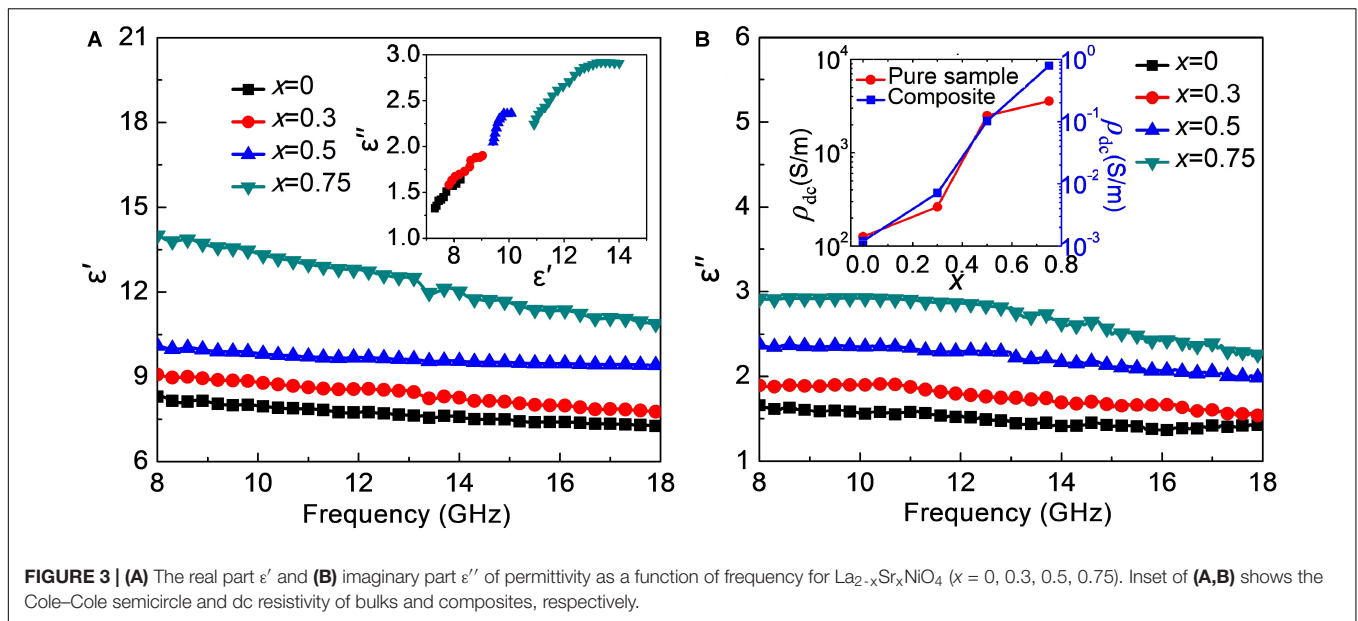
for both lattice constant a and c . The calculated refinement agrees well with the observed profiles, as shown in **Figure 1B**. As depicted in tetragonal $I4/mmm$ mode, La/Sr and O2 atoms are located at the $4e$ ($0, 0, z$) site, and Ni at $2a$ ($0, 0, 0$) and O1 at $4c$ ($0, 0.5, 0$) position, respectively (Liu et al., 2009; Chouket et al., 2016a). The stability of $\text{La}_{2-x}\text{Sr}_x\text{NiO}_{4\pm\delta}$ with the K_2NiF_4 -type structure can be evaluated in terms of the Goldschmidt tolerance factor t (Goldschmidt, 1926). The tolerance factor t ranging over 0.88–0.99 reflects the stable structure (Ganguly and Rao, 1984). According to Shannon's ionic radii ($r\text{La}^{3+} = 1.216 \text{ \AA}$, $r\text{Sr}^{2+} = 1.31 \text{ \AA}$, $r\text{Ni}^{3+} = 0.56 \text{ \AA}$, and $r\text{O}^{2-} = 1.40 \text{ \AA}$), the calculated tolerance factors lie in the tetragonal symmetry stability interval, confirming the tetragonal symmetry of the investigated phases. Similar results were also reported in Nd-modified $\text{La}_{2-x}\text{Nd}_x\text{SrFeO}_4$ (Singh et al., 2014). The stable $\text{La}_{2-x}\text{Sr}_x\text{NiO}_4$ nickelate displays a quasi-two-dimensional structure in perovskite blocks, whose one rock salt-type (La–Sr/O) layer is sandwiched by one-octahedra-thick layer along the c axis. Besides, the interatomic distances were calculated partially for each compound, as listed in **Table 1**. Due to the closely related electromagnetic property, the evolution of bond length was discussed in subsequent analysis.

Figure 2 presents the SEM morphology of $\text{La}_{2-x}\text{Sr}_x\text{NiO}_{4\pm\delta}$ ceramics for $x = 0.0$, $x = 0.5$, and $x = 0.75$ samples. Well-crystallized and dense microstructure with an average grain size of $0.5\text{--}0.9 \mu\text{m}$ are observed. With increasing Sr content, there is no significant change in grain size. To confirm chemical composition, a quantitative elemental analysis was carried out by EDS microprobe, shown in the inset of **Figures 2a–c**. Deductively, the collected chemical composition of different grains agrees with the stoichiometric proportion and no other elements are recorded, which confirms the results found by XRD. The corresponding relative densities for $\text{La}_{2-x}\text{Sr}_x\text{NiO}_{4\pm\delta}$ ($x = 0, 0.3, 0.5, 0.75$) ceramics are 92.21, 92.77, 93.01, and 92.66% of the theoretical densities, respectively. These recording densities are high compared to that of Mn-substituted LaSrNiO_4 nickelates (88.6–92.6%) prepared by solid-state reaction material consolidated at 1300°C for heat

TABLE 1 | Structural parameters of $\text{La}_{2-x}\text{Sr}_x\text{NiO}_4$ ($x = 0, 0.3, 0.5, 0.75$) resulting from Rietveld refinements of X-ray powder diffraction.

$\text{La}_{2-x}\text{Sr}_x\text{NiO}_4$		$x = 0.0$	$x = 0.3$	$x = 0.5$	$x = 0.75$
Crystal structure		$I4/mmm$	$I4/mmm$	$I4/mmm$	$I4/mmm$
Lattice parameter	a (\AA)	3.854 (8)	3.877 (5)	3.884 (2)	3.889 (2)
	c (\AA)	12.672 (3)	12.681 (7)	12.689 (8)	12.692 (7)
	Cell volume (\AA^3)	188.221 (6)	190.609 (7)	191.419 (6)	191.957 (6)
R factors	$Z_{\text{La/Sr}}$	0.367 (4)	0.366 (3)	0.364 (7)	0.363 (3)
	R_p (%)	3.28	4.01	3.76	3.44
	wR_p (%)	5.63	5.45	5.58	5.63
	χ^2 (%)	1.77	2.06	1.86	1.49
Bond length	Ni–O(1) (\AA)	1.936 (3)	1.932 (5)	1.930 (8)	1.929 (9)
	Ni–O(2) (\AA)	2.309 (7)	2.288 (7)	2.271 (5)	2.260 (1)
	La(Sr)–O(1)	2.634 (5)	2.619 (5)	2.604 (3)	2.588 (5)
	La(Sr)–O(2a)	2.339 (7)	2.355 (3)	2.379 (4)	2.398 (7)
	La(Sr)–O(2b)	2.779 (9)	2.788 (11)	2.794 (11)	2.801 (9)
Tolerance factor t		0.944	0.954	0.961	0.969



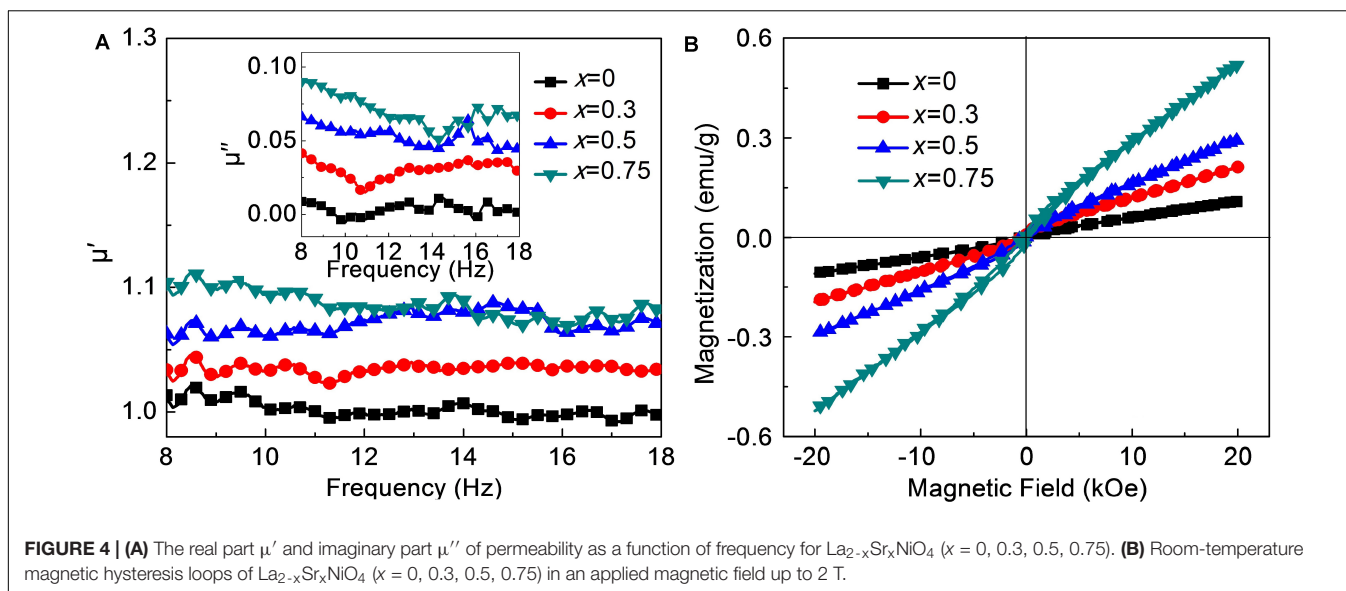


preservation at 8 h (Chouket et al., 2016b), manifesting the sol-gel route and providing dense and pure microstructure at lower sintering temperature in a shorter time.

Figure 3 displays the frequency-dependent complex permittivity with different Sr doping levels in the frequency range of 8–18 GHz. Evidently, the real part ϵ' of permittivity in composites is highly sensitive to the strontium substitution. ϵ' climbs with the increasing Sr concentration. For example, the ϵ' increases with values up to 8.97, 9.83, and 13.36 for $x = 0.3$, $x = 0.5$, and $x = 0.75$ at 10 GHz, respectively, which are higher than that in the pure sample ($\epsilon' \sim 7.98$). This increased ϵ' in Sr-substituted $\text{La}_{2-x}\text{Sr}_x\text{NiO}_{4\pm\delta}$ is related to the intrinsic polarization and charge ordering. The substitution of La with Sr renders the distortion of $(\text{La}/\text{Sr})\text{O}_9$ dodecahedra with changed cation–oxygen bond length. As listed in **Table 1**, the release of the compressed $(\text{La}/\text{Sr})\text{O}(2b)$ bond and the elongation of the $(\text{La}/\text{Sr})\text{O}(2a)$ bond break the original non-polarity-forming dipoles. Therefore, the electromagnetic field triggers dipoles to reorient field direction, promoting intrinsic orientational polarization. Furthermore, localized stripe-like charge carriers hopping between spatially fluctuating lattice induce the occurrence of dipolar and inhomogeneous charge distribution in the La_2NiO_4 system (Sachan et al., 1995). On account of the low strontium doping level and oxygen non-stoichiometry in the lattice, the nickel mostly appears in the Ni^{2+} state in $\text{La}_{2-x}\text{Sr}_x\text{NiO}_{4\pm\delta}$ (Poirot et al., 2008). An expansion of the lattice parameter after introducing large ionic would lead to the creation of Ni^{3+} ions in the lattice. The electromagnetic field causes the $\text{Ni}^{2+}\text{--Ni}^{3+}$ dipole reorientation and rearrangement. Therefore, the presence of charge hopping between the dipoles contributes to the dielectric response. From the inset of **Figure 3A**, the distorted Cole–Cole semicircles in the ϵ' vs. ϵ'' curve correspond to the existence of a dielectric relaxation process and confirm the dipole polarization contributing to permittivity at microwave frequency (Wen et al., 2013).

The ϵ'' curves shift upward compared with the unsubstituted La_2NiO_4 in the investigated frequency range. This increased ϵ'' stems mainly from strengthened conductance in nickelate, following the relation $\epsilon'' = \sigma/2\pi f\epsilon_0$. As shown in the inset of **Figure 3B**, the conductivity increases near two orders of magnitude than the free doped sample in compounds. The increased conductivity derives from the contraction of the Ni–O1 equatorial bond lengths, as described in **Table 1**, which induced a large number of charge carriers in the conduction band upon hole injection (Aguadero et al., 2006). With increasing Sr-doping level, the hole injection effect causes more covalence and the shorter Ni–O chemical bonds with a higher transfer integral, yielding a strengthened charge transport across the solid. As discussed previously, electrical conductivity plays a key role in dielectric absorbent, which contributes to the transmission of microwave energy to heat energy from the enhancement of induced microcurrent. Based on the measured conductivity result in composites, the electrical conductivity approaches 1 S/m in $\text{La}_{2-x}\text{Sr}_x\text{NiO}_{4\pm\delta}$ compounds ($x = 0.75$). Meanwhile, the real permittivity ϵ' of composites seems to remain in the range 10–15 within the whole investigated frequency window, while the ϵ'' is close to 3 in the frequency range 8–13 GHz. This combination of appropriate dielectric constant and electrical conductivity is favorable to microwave absorbing performance.

Figure 4A depicts the frequency-dependent real part μ' and imaginary part μ'' of permeability for $\text{La}_{2-x}\text{Sr}_x\text{NiO}_{4\pm\delta}$ ($x = 0, 0.3, 0.5, 0.75$) in the frequency range of 8–18 GHz. The permeability of all samples has been found to be undulating slightly. The nickelates show unsaturation at a magnetic field of 20 kOe magnetization and ignorable coercivity, consistent with the behavior in magnetization measurements (Cava et al., 1991). Comparatively, by introducing Sr in La_2NiO_4 , both the real part μ' and imaginary part μ'' show an apparent increment in investigated frequency window. The increased μ' in doped samples depends mainly on the increased saturation



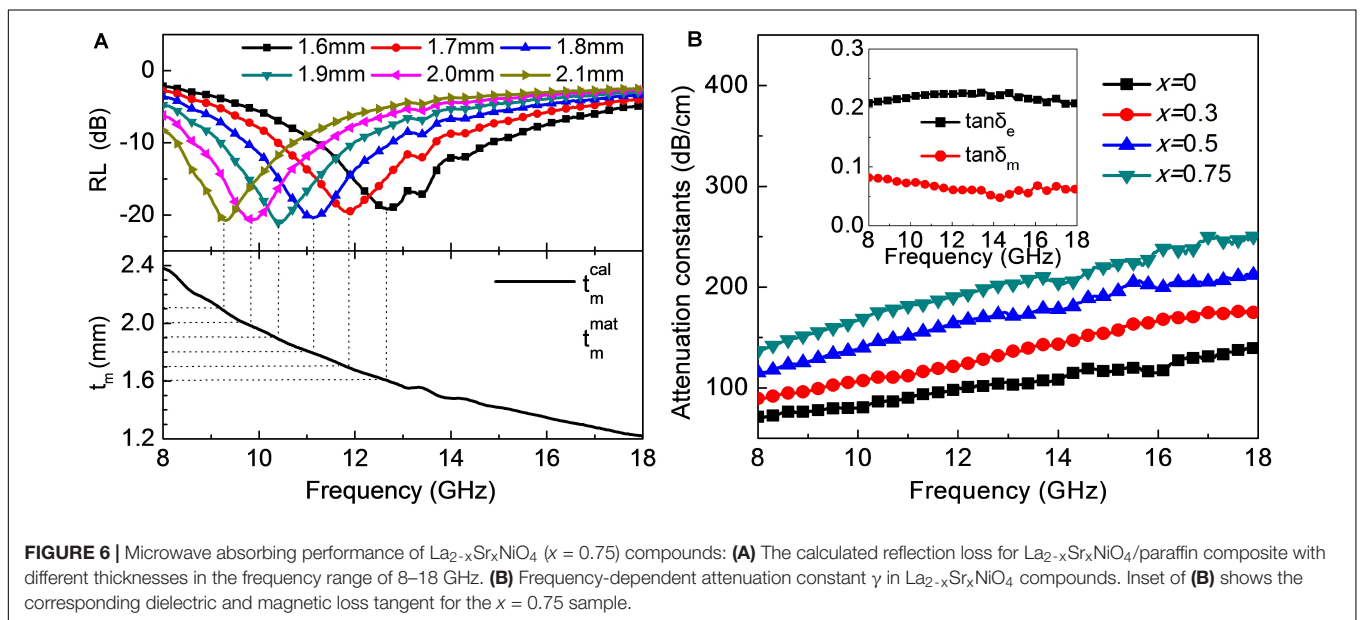
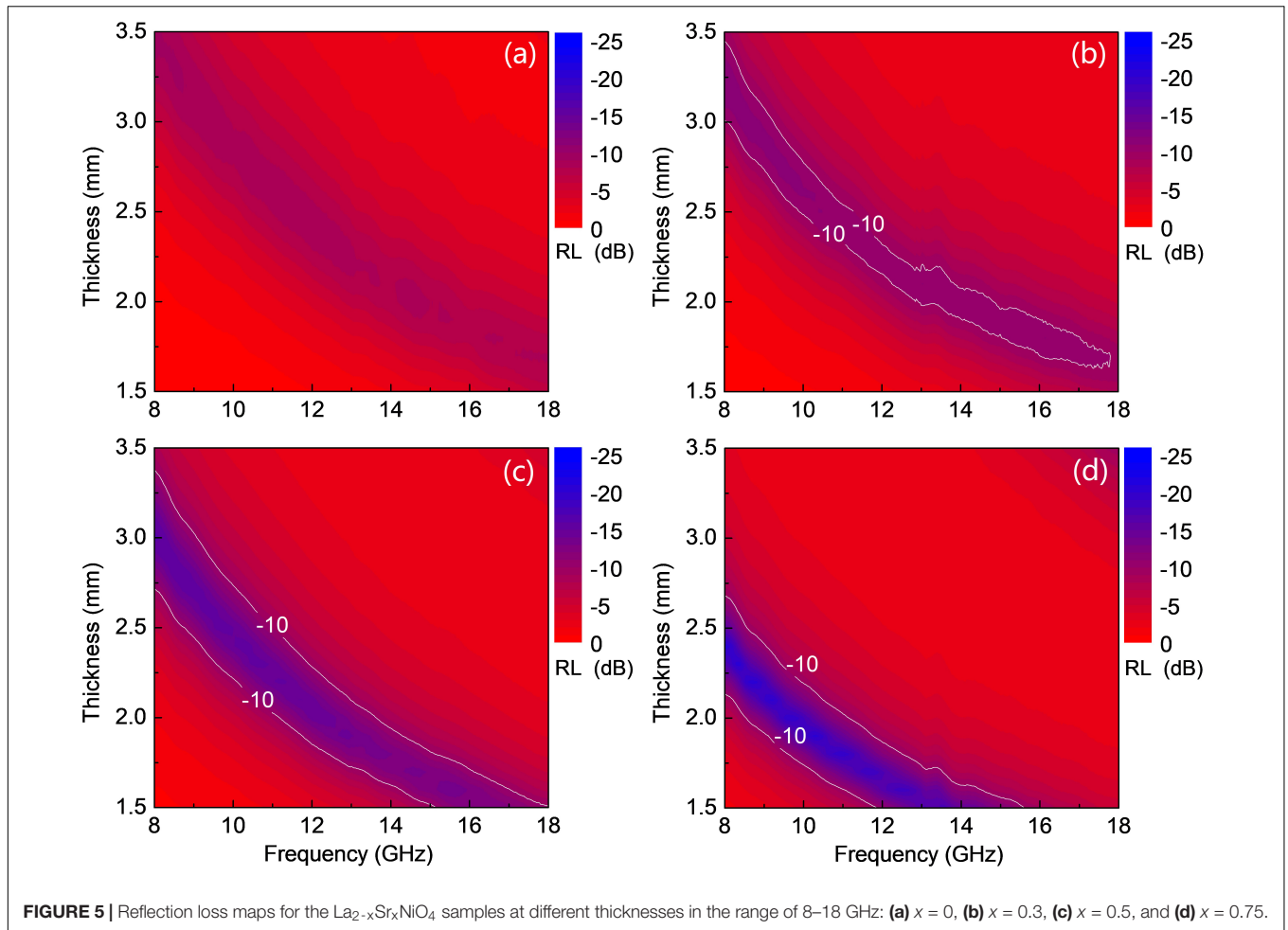
magnetization, as shown in **Figure 4B**. The induced weak magnetic moment increases almost linearly with field strength, indicating that the $\text{La}_{2-x}\text{Sr}_x\text{NiO}_{4\pm\delta}$ exhibits paramagnetic behavior. The doping effect leads to an enhanced spontaneous magnetization and was found to maximize at $x = 0.75$ with the value of 0.52 emu/g. Similar results are observed in the divalent Sr-doped compound BiFeO_3 (Chauhan et al., 2016). In the case of Sr-doped $\text{La}_{2-x}\text{Sr}_x\text{NiO}_{4\pm\delta}$, the canting of Ni spins caused by the structural distortion might be responsible for the improved magnetization. The Sr substitution for La in $\text{La}_{2-x}\text{Sr}_x\text{NiO}_{4\pm\delta}$ compounds is charge-compensated by the generation of extra holes, resulting from the transformation of Ni^{2+} to Ni^{3+} (Klingeler et al., 2005; Tran et al., 2013). Hence, the presence of interactions of $\text{Ni}^{2+}-\text{Ni}^{2+}$ and $\text{Ni}^{2+}-\text{Ni}^{3+}$ enhances the magnetic properties. From the inset of **Figure 4A**, the slightly increased μ'' brings microwave attenuation.

According to Eqs. (1) and (2), the RL map of the $\text{La}_{2-x}\text{Sr}_x\text{NiO}_{4\pm\delta}$ ($x = 0, 0.3, 0.5, 0.75$) composites in 8–18 GHz covering the thickness range 1.5–3.5 mm is simulated and illustrated in **Figure 5**. It is found that the microwave attenuation ability and absorption bandwidth of La_2NiO_4 are significantly enhanced by Sr modification. Pristine La_2NiO_4 obtains the maximum absorption peak of -9.28 dB (~88.19% absorption) in the investigated frequency range at a thickness of 3.3 mm. Note that the sample $x = 0.75$ exhibits a strong intensity of -21.04 dB (~99.21% absorption) at a small thickness of 1.9 mm, covering an effective absorption bandwidth (RL < -10) of 2.9 GHz (9.1–12.0 GHz). Compared to that of pure La_2NiO_4 , composites exhibit a broadened effective absorption bandwidth, confirming that composition modification is helpful to attenuate microwave energy here. The absorption bandwidth and matching thickness in $\text{La}_{1.25}\text{Sr}_{0.75}\text{NiO}_{4\pm\delta}$ are superior to those reported in $\text{La}_{1.5}\text{Sr}_{0.5}\text{NiO}_{4\pm\delta}$ ultrafine particles (1.4 GHz and 3.0 mm) (Tho et al., 2014) and the $0.4\text{CoFe}_2\text{O}_4-0.6\text{La}_{1.5}\text{Sr}_{0.5}\text{NiO}_{4\pm\delta}$ composite (2.6 GHz and 2.5 mm) (Xuan et al., 2014).

Figure 6A shows the calculated RL of composites over 8–18 GHz at six typical values of thickness from 1.6 to 2.1 mm for the $x = 0.75$ compound. As clearly seen, the optimal absorption peak downshifts to low frequency from 12.7 to 9.1 GHz when the absorption layer gets thicker. Such peak shifting can be reasonably described by the quarter-wave matching model $f_r = c/4t_{\text{calm}} \cdot (\mu_r \cdot \epsilon_r)^{1/2}$ (Liu et al., 2019), where t_{calm} and f_r are the matching thickness and frequency of minimum RL peaks and c represents the velocity of light in vacuum. The calculated thickness t_{calm} shown in **Figure 6A** agrees well with the matching thickness t_{matm} . Since the microwave absorption performance of MAMs is closely determined by the microwave attenuation ability, the attenuation characteristics of Sr-substituted La_2NiO_4 particulate-paraffin composites were established. The inset of **Figure 6B** illustrates the frequency-dependent dielectric loss tangent ($\tan\delta_e = \epsilon''/\epsilon'$) and the magnetic loss tangent ($\tan\delta_m = \mu''/\mu'$) for the $x = 0.75$ sample. The frequency-dependent dielectric and magnetic losses exhibit an almost reverse tendency. Further, the larger $\tan\delta_e$ than $\tan\delta_m$ indicates that the main contribution of the attenuation capability comes from the high dielectric loss. The attenuation ability can also be evaluated by the attenuation constant γ , given as (Fang et al., 2016; Liu et al., 2019):

$$\gamma = \frac{2\pi f}{c} \sqrt{(\mu''\epsilon'' - \mu'\epsilon') + \sqrt{(\mu''\epsilon'' - \mu'\epsilon')^2 + (\mu'\epsilon'' + \mu''\epsilon')^2}} \quad (3)$$

Attenuation constant γ displays the absorption ability of EM wave entering the absorber. The greater the value, the more effective would be the dissipation with short propagation distance. From **Figure 6B**, the Sr-substituted sample displays a large γ value in the whole investigated frequency range compared to the undoped one, especially the highly doped samples with high ϵ'' . Also, the change trend of γ along with substitution content are in accord with the RL in **Figure 5**. According to the measured electromagnetic parameters, one can reasonably



infer that a large imaginary part of the electromagnetic parameter mainly contributes to the attenuation constant γ .

Based on the analysis above, more attention should be paid on the dielectric loss characteristic for the Sr-substituted $\text{La}_{2-x}\text{Sr}_x\text{NiO}_{4\pm\delta}$ nickelate. As illustrated in **Figure 3**, the enhanced microwave absorption performance should point to the dielectric properties. The augmentative electrical conductivity proves to be beneficial for composites. The Sr-modified nickelate composite effectively increases the electrical conductivity of the pristine La_2NiO_4 composite (**Figure 3B**). As a result, a large conductance loss within highly conductive layers allows electromagnetic energy conversion. Thus, it is expected that the Sr-doped nickelate could be a promising high-performance microwave absorbent. Besides, since electromagnetic absorbing loss stems mainly from the polarization relaxation within grains and between grain boundaries, more grain boundaries contribute to interfacial polarization and alter dielectric response. According to the microtopography in **Figure 2**, there is no significant change in grain size with varying Sr content. In our case, we mainly focus on the relationship between Sr doping content and electromagnetic properties in La_2NiO_4 nickelate. Further studies on size effect are necessary and will be performed in our future work on modified samples.

CONCLUSION

In this paper, we have demonstrated the enhanced microwave absorbing performance of Sr-modified $\text{La}_2\text{NiO}_{4\pm\delta}$ nickelate by analyzing the effect of Sr substitution on structure, conductive, and dynamic electromagnetic properties. The sol-gel-prepared Sr-modified $\text{La}_2\text{NiO}_{4\pm\delta}$ compounds reveal a pure and dense microstructure. The electromagnetic response of doped samples exhibits associativity with the changed crystal structure. The

REFERENCES

- Aguadero, A., Escudero, M. J., Perez, M., Alonso, J. A., Pomjakushin, V., and Daza, L. (2006). Effect of Sr content on the crystal structure and electrical properties of the system $\text{La}_{2-x}\text{Sr}_x\text{NiO}_{4+\delta}$ ($0=x=1$). *Dalton Trans.* 36, 4377–4383. doi: 10.1039/b606316k
- Bollen, P., Quievry, N., Huynen, I., Bailly, C., Detrembleur, C., Thomassin, J. M., et al. (2013). Multifunctional architected materials for electromagnetic absorption. *Scr. Mater.* 68, 50–54. doi: 10.1016/j.scriptamat.2012.05.011
- Cava, R. J., Batlogg, B., Palstra, T. T., Krajewski, J. J., Peck, W. F. Jr., Ramirez, A. P., et al. (1991). Magnetic and electrical properties of $\text{La}_{2-x}\text{Sr}_x\text{NiO}_{4\pm\delta}$. *Phys. Rev. B* 43, 1229–1232.
- Chauhan, S., Kumar, M., and Pal, P. (2016). Substitution driven structural and magnetic properties and evidence of spin phonon coupling in Sr-doped BiFeO_3 nanoparticles. *RSC Adv.* 6, 68028–68040. doi: 10.1039/c6ra11021e
- Chen, J., Liang, X., Liu, W., Gu, W., Zhang, B., and Ji, G. (2019). Mesoporous carbon hollow spheres as a light weight microwave absorbing material showing modulating dielectric loss. *Dalton Trans.* 48, 10145–10150. doi: 10.1039/c9dt01876j
- Chen, M., Yu, H., Jie, X., and Lu, Y. (2018). Optimization on microwave absorbing properties of carbon nanotubes and magnetic oxide composite materials. *Appl. Surf. Sci.* 434, 1321–1326. doi: 10.1016/j.apsusc.2017.11.107

Sr-doped nickelates were experimentally found to increase high dielectric, which provides a large attenuation ability for microwave absorbing. Accordingly, an optimal RL of -21.07 dB could be achieved with a broad range of 2.9 GHz at a small thickness of 1.9 mm. This enhanced microwave absorbing performance in nickelates expands its application field.

DATA AVAILABILITY STATEMENT

The raw data supporting the conclusions of this article will be made available by the authors, without undue reservation, to any qualified researcher.

AUTHOR CONTRIBUTIONS

SL made substantial contributions to the conception and design of the work. SL and JH made substantial contributions to the acquisition, analysis, and interpretation of data for the work and agreed to be accountable for all aspects of the work in ensuring that questions related to the accuracy or integrity of any part of the work were appropriately investigated and resolved. SL, JH, and SY drafted the work. HL and YC revised it critically for important intellectual content. LD approved the final version to be published. All authors contributed to the article and approved the submitted version.

FUNDING

This work was financially supported by the National Natural Science Foundation of China (51902104) and the National Key Research and Development Program of China (2017YFA0204600).

- Chen, S., Tan, G., Gu, X., Man, Q., Li, F., Chang, C., et al. (2017). Microwave absorbing properties of FeCrMoNiPBCSi amorphous powders composite. *J. Alloys Compd.* 705, 309–313. doi: 10.1016/j.jallcom.2017.02.089
- Chouket, A., Bidault, O., Optasanu, V., Cheikhrouhou, A., Cheikhrouhou-Koubaa, W., and Khitouni, M. (2016a). Enhancement of the dielectric response through Al-substitution in $\text{La}_{1.6}\text{Sr}_{0.4}\text{NiO}_4$ nickelates. *RSC Adv.* 6, 24543–24548. doi: 10.1039/c5ra27071e
- Chouket, A., Optasanu, V., Bidault, O., Cheikhrouhou, A., Cheikhrouhou-Koubaa, W., and Khitouni, M. (2016b). Dielectric relaxation and polaronic hopping in Mn-substituted LaSrNiO_4 nickelates prepared by mechanical milling method. *J. Alloys Compd.* 688, 163–172. doi: 10.1016/j.jallcom.2016.06.288
- Duan, G., Liu, S., Jiang, S., and Hou, H. (2019). High-performance polyamide-imide films and electrospun aligned nanofibers from an amide-containing diamine. *J. Mater. Sci.* 54, 6719–6727. doi: 10.1007/s10853-019-03326-w
- Duan, W., Yin, X., Li, Q., Schlier, L., Greil, P., and Travitzky, N. (2016). A review of absorption properties in silicon-based polymer derived ceramics. *J. Eur. Ceram. Soc.* 36, 3681–3689. doi: 10.1016/j.jeurceramsoc.2016.02.002
- Fang, J., Liu, T., Chen, Z., Wang, Y., Wei, W., Yue, X., et al. (2016). A wormhole-like porous carbon/magnetic particles composite as an efficient broadband electromagnetic wave absorber. *Nanoscale* 8, 8899–8909. doi: 10.1039/c6nr01863g
- Feng, W., Luo, H., Wang, Y., Zeng, S., Tan, Y., Deng, L., et al. (2019). Mxenes derived laminated and magnetic composites with excellent microwave absorbing performance. *Sci. Rep.* 9:3957.

- Freeman, P. G., Giblin, S. R., Hradil, K., Mole, R. A., Cermak, P., and Prabhakaran, D. (2017). Magnetic excitations of the charge stripe electrons below half doping in $\text{La}_{2-x}\text{Sr}_x\text{NiO}_4$ ($x=0.45, 0.4$). *Phys. Rev. B* 95:064403.
- Ganguly, P., and Rao, C. N. R. (1984). Crystal chemistry and magnetic properties of layered metal oxides possessing the K_2NiF_4 or related structures. *J. Solid State Chem.* 53, 193–216. doi: 10.1016/0022-4596(84)90094-x
- Goldschmidt, V. M. (1926). *Skrifter Norske Videnskaps-Akad.* Oslo: Naturwiss. Klasse No. 8.
- He, J., Luo, H., He, L. H., Yan, S. Q., Shan, D. Y., Huang, S. X., et al. (2011). Investigation on microwave dielectric behavior of flaky carbonyl iron composites. *J. Mater. Sci. Mater. Electron.* 29, 15112–15118. doi: 10.1007/s10854-018-9652-5
- Huynen, I., Quievy, N., Bailly, C., Bollen, P., Detrembleur, C., Eggermont, S., et al. (2011). Multifunctional hybrids for electromagnetic absorption. *Acta. Mater.* 59, 3255–3266. doi: 10.1016/j.actamat.2011.01.065
- Jiang, S., Cheong, J. Y., Nam, J. S., Kim, I., Agarwal, S., and Greiner, A. (2020). High-density fibrous polyimide sponges with superior mechanical and thermal properties. *ACS Appl. Mat. Interfaces* 12, 19006–19014. doi: 10.1021/acsami.0c02004
- Klingeler, R., Buechner, B., Cheong, S. W., and Huecker, M. (2005). Weak ferromagnetic spin and charge stripe order in $\text{La}_5/3\text{Sr}_1/3\text{NiO}_4$. *Phys. Rev. B* 72:104424.
- Kong, L., Yin, X., Ye, F., Li, Q., Zhang, L., and Cheng, L. (2013). Electromagnetic wave absorption properties of ZnO-Based materials modified with ZnAl_2O_4 nanograins. *J. Phys. Chem. C* 117, 2135–2146. doi: 10.1021/jp309984p
- Krohns, S., Lunkenheimer, P., Kant, Ch, Pronin, A. V., Brom, H. B., Nugroho, A. A., et al. (2009). Colossal dielectric constant up to gigahertz at room temperature. *Appl. Phys. Lett.* 94, 122903–122903-3.
- Larson, A. C., and Von Dreele, R. B. (2004). *General Structure Analysis System (GSAS)*. Los Alamos National Laboratory Report LAUR 86–748. Los Alamos, NM: Los Alamos National Laboratory
- Liao, X., Ye, W., Chen, L., Jiang, S., Wang, G., Zhang, L., et al. (2017). Flexible hdC -G reinforced polyimide composites with high dielectric permittivity. *Compos. Part A Appl. S.* 101, 50–58. doi: 10.1016/j.compositesa.2017.06.011
- Liu, S., Wei, K., Cheng, Y., Yan, S., He, L., and Deng, L. (2019). Structural, magnetic and microwave electromagnetic properties in La substituted quaternary ferrite. *J. Alloys Compd.* 791, 469–476. doi: 10.1016/j.jallcom.2019.03.227
- Liu, X. Q., Wu, Y. J., Chen, X. M., and Zhu, H. Y. (2009). Temperature-stable giant dielectric response in orthorhombic samarium strontium nickelate ceramics. *J. Appl. Phys.* 105:054104. doi: 10.1063/1.3082034
- Luo, H., Feng, W., Liao, C., Deng, L., Liu, S., Zhang, H., et al. (2018). Peaked dielectric responses in Ti_3C_2 MXene nanosheets enabled composites with efficient microwave absorption. *J. Appl. Phys.* 123:104103. doi: 10.1063/1.5008323
- Poirot, N., Simon, P., and Odier, P. (2008). Anomalies of ESR spectra of the $\text{La}_2\text{NiO}_4+\delta$ system. *Solid State Sci.* 10, 186–192. doi: 10.1016/j.solidstatesciences.2007.08.015
- Qi, X., Hu, Q., Xu, J., Xie, R., Bai, Z., Jiang, Y., et al. (2016). Enhanced microwave absorption properties and mechanism of core/shell structured magnetic nanoparticles/carbon-based nanohybrids. *Mater. Sci. Eng. B* 211, 53–60. doi: 10.1016/j.mseb.2016.05.018
- Rivas, J., Rivas-Murias, B., Fondado, A., Mira, J., and Senaris-Rodriguez, M. A. (2004). Dielectric response of the charge-ordered two-dimensional nickelate $\text{La}_{1.5}\text{Sr}_{0.5}\text{NiO}_4$. *Appl. Phys. Lett.* 85, 6224–6226. doi: 10.1063/1.1834998
- Ruddlesden, S. N., and Popper, P. (1957). New compounds of the K_2NiF_4 -type. *Acta Crystallogr.* 10, 538–539.
- Sachan, V., Buttrey, D. J., Tranquada, J. M., Lorenzo, J. E., and Shirane, G. (1995). Stoichiometry, structure, and properties of $\text{La}_2\text{NiO}_4+\delta$ and $\text{La}_{2-x}\text{Sr}_x\text{NiO}_4\pm\delta$. *Phys. Rev. B* 51:12742.
- Shang, T., Lu, Q., Chao, L., Qin, Y., Yun, Y., and Yun, G. (2018). Effects of ordered mesoporous structure and La-doping on the microwave absorbing properties of CoFe_2O_4 . *Appl. Surf. Sci.* 434, 234–242. doi: 10.1016/j.apsusc.2017.10.175
- Shannon, R. D. (1976). Revised effective ionic radii and systematic studies of interatomic distances in halides and chalcogenides. *Acta Crystallogr. A* 32, 751–767. doi: 10.1107/s0567739476001551
- Shen, P., Luo, J., Zuo, Y., Yan, Z., and Zhang, K. (2017). Effect of La-Ni substitution on structural, magnetic and microwave absorption properties of barium ferrite. *Ceram. Int.* 43, 4846–4851. doi: 10.1016/j.ceramint.2016.12.107
- Singh, D., Singh, S., Mahajan, A., and Choudhary, N. (2014). Effect of substitution of magnetic rare earth Nd at non-magnetic La site on structure and properties of LaSrFeO_4 . *Ceram. Int.* 40, 1183–1188. doi: 10.1016/j.ceramint.2013.07.003
- Tho, P. T., Xuan, C. T. A., Quang, D. M., Bach, T. N., Thanh, T. D., Le, N. T. H., et al. (2014). Microwave absorption properties of dielectric $\text{La}_{1.5}\text{Sr}_{0.5}\text{NiO}_4$ ultrafine particles. *Mater. Sci. Eng. B* 186, 101–105. doi: 10.1016/j.mseb.2014.03.015
- Tran, D. T., Vu, D. L., Le, V. H., Phan, T. L., and Yu, S. C. (2013). Spin reorientation and giant dielectric response in multiferroic $\text{La}_{1.5}\text{Sr}_{0.5}\text{NiO}_4+\delta$. *Adv. Nat. Sci.: Nanosci. Nanotechnol.* 4:025010. doi: 10.1088/2043-6262/4/2/025010
- Wang, Y., Du, Y., Xu, P., Qiang, R., and Han, X. (2017). Recent advances in conjugated polymer-based microwave absorbing materials. *Polymers* 9:29. doi: 10.3390/polym9010029
- Wei, H., Yin, X., Hou, Z., Jiang, F., Xu, H., Li, M., et al. (2018). A novel SiC -Based microwave absorption ceramic with Sc_2SiO_7 as transparent matrix. *J. Eur. Ceram. Soc.* 38, 4189–4197. doi: 10.1016/j.jeurceramsoc.2018.05.005
- Wen, B., Cao, M. S., Hou, Z. L., and Song, W. L. (2013). Temperature dependent microwave attenuation behavior for carbon-nanotube/silica composites. *Carbon* 65:124. doi: 10.1016/j.carbon.2013.07.110
- Wu, G., and Neumeier, J. J. (2003). Small polaron transport and pressure dependence of the electrical resistivity of $\text{La}_{2-x}\text{Sr}_x\text{NiO}_4$ ($0=x=1.2$). *Phys. Rev. B* 67:125116.
- Xuan, C. T. A., Tho, P. T., Quang, D. M., Bach, T. N., Thanh, T. D., Le, N. T. H., et al. (2014). Microwave absorption in $\text{La}_{1.5}\text{Sr}_{0.5}\text{NiO}_4/\text{CoFe}_2\text{O}_4$ nanocomposites. *IEEE T. Magn.* 50, 1–4.
- Zhou, Y., Lü, Z., Xu, S., Xu, D., and Wei, B. (2016). Investigation of a solid oxide fuel cells catalyst LaSrNiO_4 : Electronic structure, surface segregation, and oxygen adsorption. *Int. J. Hydrogen Energ.* 41, 21497–21502. doi: 10.1016/j.ijhydene.2016.09.208

Conflict of Interest: The authors declare that the research was conducted in the absence of any commercial or financial relationships that could be construed as a potential conflict of interest.

Copyright © 2020 Liu, Cheng, He, Yan, Luo and Deng. This is an open-access article distributed under the terms of the Creative Commons Attribution License (CC BY). The use, distribution or reproduction in other forums is permitted, provided the original author(s) and the copyright owner(s) are credited and that the original publication in this journal is cited, in accordance with accepted academic practice. No use, distribution or reproduction is permitted which does not comply with these terms.